Structural and chemical determination of the new nanolaminated carbide Mo2Ga2C from first principles and materials analysis

Chung-Chuan Lai, Rahele Meshkian, Martin Dahlqvist, Jun Lu, Lars-Åke Näslund, O. Rivin, E. N. Caspi, O. Ozeri, Lars Hultman, Per Eklund, Michel Barsoum and Johanna Rosén

Linköping University Post Print

N.B.: When citing this work, cite the original article.

Structural and chemical determination of the new nanolaminated carbide Mo$_2$Ga$_2$C from first principles and materials analysis

C.-C. Lai [a], R. Meshkian [a], M. Dahlqvist [a], J. Lu [a], L.-Å. Näslund [a], O. Rivin [b], E.N. Caspi [b], O. Ozeri [c], L. Hultman [a], P. Eklund [a], M.W. Barsoum [a,d,*], J. Rosen [a,*]

[a] Thin Film Physics Division, Department of Physics, Chemistry, and Biology (IFM), Linköping University, Linköping SE-58183, Sweden

[b] Physics Department, Nuclear Research Centre-Negev, P.O. Box 9001, Beer-Sheva 84190, Israel

[c] Reactor Department, Nuclear Research Center-Soreq, Yavne 81800, Israel

[d] Department of Materials Science and Engineering, Drexel University, PA 19104, United States

* Corresponding authors at: Department of Materials Science and Engineering, Drexel University, PA 19104, United States (M.W. Barsoum), and Thin Film Physics Division, Department of Physics, Chemistry, and Biology (IFM), Linköping University, Linköping SE-58183, Sweden (J. Rosen). E-mail addresses: barsoumw@drexel.edu (M.W. Barsoum), johro@ifm.liu.se (J. Rosen).

Abstract

Following our recent discovery of a new nanolaminated carbide, Mo_2Ga_2C, we herein present a detailed structural and chemical analysis of this phase based on ab initio calculations, X-ray photoelectron spectroscopy, high resolution scanning transmission electron microscopy, and neutron powder diffraction. Calculations suggest an energetically and dynamically stable structure for C in the octahedral sites between the Mo layers, with Ga bilayers – stacked in a simple hexagonal arrangement – between the Mo_2C layers. The predicted elastic properties are below those of the related nanolaminate Mo_2GaC. The predicted structure, including lattice parameters and atomic positions, is experimentally confirmed.

1. Introduction

The $M_{n+1}AX_n$ (MAX) phases, with $n = 1–3$, are inherently nanolaminated materials, where M is an early transition metal, A is an A-group element (mainly group 13 or 14), and X is C or N [1–4]. Structurally, the MAX phases can be described as $M_{n+1}X_n$ layers interleaved by monolayers of pure A element, for which two adjacent $M_{n+1}X_n$ layers are twinned across it. So far, more than 70 MAX phases have been synthesized. Before the late 2000s most predictions were carried out in an ad hoc fashion due to a lack of a comprehensive understanding of the respective material systems [5–8]. It is not until the last few years that the theoretical methods have been more systematic, which in turn provides better guidance for experimentalists to look for new MAX phases, see e.g. references [9–12].

Recently, we reported on a new ternary carbide, Mo_2Ga_2C, both in thin film and bulk form [13]. Similar to its MAX phase counterpart, Mo_2GaC, Mo_2Ga_2C is laminated, but instead of Ga monolayers interleaving the Mo_2C blocks, there is a Ga double-layer (bilayer) between the carbide layers. The resulting phase is of great interest because of its structural similarity with

2

Mo$_2$GaC, which is the only Mo-containing MAX phase synthesized so far. Other conceivable MAX phases within the Mo–Ga–C system are predicted to be not stable, i.e. positive formation enthalpy, with respect to their competing phases [14].

In our previous report, structural and compositional analysis of Mo$_2$Ga$_2$C was performed by X-ray diffraction (XRD), transmission electron microscopy (TEM), and elastic recoil detection analysis (ERDA). However, even though we argued that the most plausible position of C in the structure was in the octahedral sites between the Mo layers, direct evidence was lacking. Quite surprisingly, the Ga layers were stacked in a simple hexagonal arrangement, one that is quite rare in metals.

The purpose of this work is to explore the structure and chemistry of Mo$_2$Ga$_2$C. We have therefore investigated the phase stability of Mo$_2$Ga$_2$C from first principles, with respect to possible competing phases in the Mo–Ga–C system, and in different structural and chemical order. We also calculated its elastic constants and electronic structure. Thermal neutron powder diffraction (NPD) was used to supplement the experimental investigation due to the sensitivity to C and Ga positions within the unit cell, in the presence of Mo atoms. Based on our theoretical modeling, combined with X-ray photoelectron spectra (XPS) and NPD, we have definitively determined the structure of this compound.

2. Computational details

First-principles calculations were carried out using the projector augmented wave (PAW) method [15] as implemented within the Vienna *ab initio* simulation package (VASP) [16–18]. We adopted the generalized gradient approximation (GGA) as parameterized by Perdew–Burke–Ernzerhof (PBE) [19] for treating electron exchange and correlation effects. Wave functions are expanded in a plane-wave basis set with an energy cutoff of 400 eV and for

3

sampling of the Brillouin zone we used the Monkhorst–Pack scheme [20]. The calculated total energy for all phases is converged to within 0.1 meV/atom in terms of k-point sampling. Structural optimizations were performed in terms of unit-cell volumes, c/a ratios (when necessary), and internal parameters to minimize the total energy.

3. Experimental details

Mo_2Ga_2C thin films were deposited by direct current magnetron sputtering (DCMS) with 3 elemental targets: Mo (Ø ≈ 7.6 cm, 99.95% purity, SCOTECH Ltd.), Ga (Ø ≈ 5.1 cm, 99.99999% purity, 5N Plus UK Ltd.) and C (Ø ≈ 7.6 cm, 99.99% purity, SCOTECH Ltd.), in ~0.5 Pa Ar with a base pressure in the range of 10^{-7} Pa. The Ga target was placed in a horizontal position, facing upwards, along the substrate normal, while the Mo and C targets were tilted 35° away from the substrate normal, co-focused on the substrate. Details about sputtering from a liquid Ga target as well as the deposition system are described elsewhere [21]. The MgO(111) substrates were cleaned sequentially in acetone, ethanol and isopropanol ultrasonic bath for 10 min each. During depositions, the substrates were kept at 560 °C and rotated at 30 rpm in order to obtain more chemically homogeneous films.

The NPD experiment was carried out at the KARL double-axis diffractometer, mounted on the Israeli Research Reactor No. 1 (IRR-1) at the Nuclear Research Center, Soreq, Israel (Israel's Atomic Energy Commission) [22]. The measurement was carried out at room temperature, with an incident neutron wavelength of 0.982(1) Å. This low incident wavelength, combined with an angular step of 0.05° and a ~0.25° monochromating single crystal's mosaicity, generated sufficient angular range and angular resolution for this crystallographic study. The preparation of Mo_2Ga_2C powder samples for the NPD experiment is described in our previous work [13]. A ~10 g powder sample was loaded into a vanadium cylindrical sample holder, which was used

to significantly reduce coherent scattering from the holder. The results obtained were analyzed using the Rietveld refinement method, applied using the FullProf software package [23].

To acquire cross-sectional images and compositional maps on thin film samples, high resolution scanning transmission electron microscopy (HR-STEM) and X-ray energy dispersive spectroscopy (EDX) were performed within the Linköping double C_s corrected FEI Titan[3] 60–300 microscope equipped with the Super-X EDX system and operated at 300 kV.

XPS on phase pure thin films was performed using an AXIS Ultra[DLD] system from Kratos and monochromatic Al K_α radiation. To avoid charging, caused by electron depletion while recording the XPS spectra, the samples were exposed to an electron flood gun. The binding energy scale of all XPS spectra presented here was calibrated against the Fermi edge (E_f), which was set to a binding energy of 0 eV. The overall energy resolution obtained was better than 0.5 eV. Normalization of all spectra was performed at the background on the low binding energy side of the main peak/-peaks. Prior to the acquisition of the spectra, the samples were exposed to an Ar^+ bombardment corresponding to 500 eV beam energy for 60 s. The Ar^+ bombardment was performed at an angle of 25° relative the surface, which efficiently removes most oxide overlayers and most of the carbon containing contamination.

4. Results and discussion

The position of carbon in the crystal structure of Mo_2Ga_2C is challenging to obtain from STEM. However, STEM images revealed a relatively large atomic spacing between two adjacent Mo layers and two adjacent Ga layers. The more likely location for the C atoms – and the one we assumed in our first report [13] – is the octahedral sites created by the Mo layers (Fig. 1(a)). Other possibilities include structures with C atoms in between the Ga layers (Fig. 1(b)) or with the C between the Mo layers, but in a 'zig-zag' arrangement of Ga layers (Fig. 1(c)).

For a phase with a given composition and structure to be thermodynamically stable, its energy needs to be lower than the energy of any stoichiometric linear combination of all other competing phases in the system, that is

$$\Delta H_{cp} = E(\text{Mo}_2\text{Ga}_2\text{C}) - E(\text{competing phases}) < 0 \qquad (1)$$

In order to identify the set of most competing phases at the $\text{Mo}_2\text{Ga}_2\text{C}$ composition we make use of a linear optimization procedure [24,25] which has proven successful in confirming already experimentally known MAX phases, as well as predicting the existence of new ones [25–27]. Table 1 lists all competing phases together with their respective calculated volume, lattice parameters, and total energies.

In Table 2, the calculated equilibrium energies and lattice parameters show that $\text{Mo}_2\text{Ga}_2\text{C}$, with C atoms between the Mo-layers (Fig. 1(a)) is the most likely structure with a calculated negative ΔH_{cp} of −9 meV/atom. The energies for the structures with either C atoms between the Ga layers (Fig. 1(b)) or C atoms between the Mo layer plus a zigzag stacking of the Ga atoms (Fig. 1(c)), are significantly higher, +786 and +124 meV/atom, respectively. The latter two structures would also have c parameters well below 18 Å, which is inconsistent with previous experimental results [13].

To further explore the various possible $\text{Mo}_2\text{Ga}_2\text{C}$ structures we calculated their phonon spectra using the Phonopy code in combination with density functional perturbation theory in VASP using $4 \times 4 \times 1$ supercells. Fig. 2(a)–(c) shows the results for the structures shown in Fig. 1(a)–(c), respectively, from which we can conclude that the structure shown in Fig. 1(a) is dynamically stable, i.e. stable relative to lattice vibrations as evidenced by the fact that no imaginary phonon frequencies exist in the phonon spectrum. When the C atoms are placed between the Ga-layers (Fig. 1(b)), the phonon spectrum (Fig. 2(b)) is negative along some

directions, confirming that this structure is dynamically unstable. The same result applies for the zig-zag stacking of Ga (Figs. 1(c) and 2(c)).

In Table 3, the calculated a and c lattice parameters and the structural model of the most stable structure (Fig. 1(a)) are summarized, together with previous results from XRD Rietveld analysis [13]. The Ga and Mo atomic arrangements are thus consistent with our previous suggestion based on STEM images acquired along the [100] and [210] zone axes of the Mo_2Ga_2C phase as well as Rietveld analysis of the XRD patterns. Furthermore, the calculated a and c lattice parameters are in good agreement with the ones obtained from XRD. The Mo double-layers, with C atoms occupying the octahedral interstitial sites, is identical to that found for the M–C layers in other M_2AX phases. In fact, the only structural difference between the M_2A_2X and M_2AX is the insertion of an extra A layer. We conclude that in Mo2Ga2C the C atoms reside between the Mo layers and that the Ga atoms are stacked in a simple hexagonal arrangement (Fig. 1(a)).

The NPD results were analyzed assuming the $P6_3/mmc$ space group, with the Mo and Ga atoms occupying the '4f' site and the C atoms occupying the '2a' site (Fig. 1(a)). The C occupancy was assumed to be incomplete within the refinement process, $Mo_2Ga_2C_{1-x}$, with x representing the deviation from complete occupation of the '2a' site. In addition to x, the refinement process yields the unit cell size parameters, the Mo and Ga layers position, z_{Mo} and z_{Ga}, within the unit cell, respectively, and their mean-square displacement (assumed to be isotropic) from equilibrium position, $\langle u^2 \rangle$, due to temperature driven vibrations, see Table 3. The refined profile agrees well with the observed results, see Fig. 3 (top), as shown by their difference, normalized by the statistical uncertainty in the observed neutron count, Stat. SD, as shown in Fig. 3 (bottom), which is randomly distributed around zero with reasonable deviations from it. The possibility of preferred orientation within the powder grains, the effect of the average powder grains size, and the possibility that the Ga atoms occupy the '4e' crystallographic site, were considered and

7

found inconsistent with the observed results. In addition, the observed low-angle count is considerably high, (see inset in Fig. 3). As this count includes the 002 reflection, it was empirically taken into account within the analysis process. We speculate that this additional count may originate from a significant variance in z_{Mo} and z_{Ga}, within each powder grain, from their mean respective values, which requires additional research.

The result from NPD Rietveld refinement, as summarized in Table 3, is in good agreement with the calculated structure as well as the XRD Rietveld analysis [13]. Apart from Table 3, the mean-square displacement $\langle u^2 \rangle$ of Mo, Ga, and C were determined to be <0.01 Å^2, ~0.03(1) Å^2, and <0.01 Å^2, respectively. Moreover, the NPD analysis shows a C occupancy deviation $|x| <$ 0.03, i.e. suggesting fully occupied octahedral sites, within the NPD precision, with C atoms between the Mo layers. This further validates our previously reported analysis and the present theoretical work, which were based on a fixed 100% C occupancy on the octahedral sites.

Fig. 4 shows the electronic band structure and density of states (DOS) for Mo$_2$Ga$_2$C. Non-bonding core states of C 2s and Ga 2s are located at −11.4 to −12.9 eV and −4 to −10 eV, respectively. Between −4.3 and −7.3 eV the Mo 4d and C 2p states form a hybridized bond. The peak around −2.5 eV shows partial hybridization of Mo 4d and Ga 4p states. Between −2.5 eV and the Fermi level (E_f) there are several peaks arising from both Mo 4d and Ga 4p states, where none show any clear hybridization between each other. The peak located just below E_f can mainly be attributed to Mo 4d states. E_f is located near a local minimum.

To obtain the elastic properties of Mo$_2$Ga$_2$C, we used the method described by Fast et al. [28], where five different strains are applied to the hexagonal unit cell in order to obtain the five independent elastic constants C_{11}, C_{12}, C_{13}, C_{33}, and C_{44}. The strain values used to calculate the elastic constants were ±0.01 and ±0.02. From the elastic constants C_{ij} it is possible to estimate the Voigt bulk (B_V) and shear (G_V) moduli given by

$$B_V = \frac{2}{9}(C_{11} + C_{12} + 2C_{13} + C_{33}/2) \qquad (2)$$

and

$$G_V = 115(2C_{11} + C_{33} - C_{12} - 2C_{13}) + 15(2C_{44} + 12(C_{11} - C_{12})) \qquad (3)$$

In addition the Young's modulus (E), Poisson's ratio (ν), and shear anisotropy factor (A) is given by

$$E = \frac{9B_V G_V}{3B_V + G_V} \qquad (4)$$

$$\nu = \frac{3B_V - 2G_V}{2(3B_V + G_V)} \qquad (5)$$

$$A = \frac{4C_{44}}{C_{11} + C_{33} - 2C_{13}} \qquad (6)$$

In Table 4, the calculated elastic properties for Mo2Ga2C are listed and compared to those of Mo_2GaC. It is evident that the additional Ga layer in Mo_2Ga_2C results in a significant reduction of most of the elastic constants, Poisson's ratio, and the anisotropy factor, A.

Fig. 5(a) is a STEM image acquired along the [210] zone axis of Mo_2Ga_2C from a thin film sample. Fig. 5(b) and (c) show Mo + Ga EDX maps (center) and superimposed STEM images with Mo + Ga EDX maps (bottom) from the same acquisition regions. In Fig. 5(a), the contrasts show a layered structure constructed by Mo layers (white) and Ga layers (light gray), which is further indicated by green 'Ga' labels. These results confirm those previously obtained [13]. What is additional here is the clear evidence for a stacking fault, where the double Ga layers of Mo_2Ga_2C merge into a single Ga layer characteristic of Mo_2GaC denoted by vertical green line in Fig. 5(a). The transition region is imaged at a higher magnification in Fig. 5(c), from which it is obvious that two Ga layers on the right merge into one on the left. In other areas (Fig. 5(b)),

9

single and double Ga layers are interleaved. In all cases, however, the Ga layers are separated by two Mo layers. The formation of such stacking faults most probably reflects local compositional Ga inhomogeneities. These micrographs suggest that one way to synthesize Mo_2Ga_2C is to anneal Mo_2GaC in a Ga-rich environment.

A comparison between the XPS results for Mo_2Ga_2C and Mo_2GaC is shown in Fig. 6, which presents the O 1s, C 1s, Mo 3d, and Ga 3p spectra for Mo_2GaC (a) and Mo_2Ga_2C (b). The O 1s and C 1s spectra show that, despite the Ar^+ bombardment, the samples still exhibit oxide and graphite components as revealed through the O 1s feature at 530.8 and 531.5 eV and the C 1s feature at 284.7 and 285.4 eV for the Mo_2GaC and Mo_2Ga_2C samples, respectively. More important, though, is the sharp carbide peaks at 283.3 and 283.7 eV for Mo_2GaC and Mo_2Ga_2C, respectively. The Mo 3d XPS spectra feature the primary spin–orbit components $3d_{5/2}$ and $3d_{3/2}$ at binding energies of 227.9 and 231.1 eV, respectively, for Mo_2GaC and at binding energies of 228.1 and 231.3 eV, respectively, for Mo_2Ga_2C. The Ga $3p_{3/2}$ and $3p_{1/2}$ components have the main features at binding energies of 104.0 and 107.1 eV, respectively, for Mo_2GaC and binding energies of 104.1 and 107.3 eV, respectively, for Mo_2Ga_2C.

To be able to interpret the XPS spectra presented in Fig. 6, it is necessary to compare them with the 3p XPS component of a metallic Ga reference. The Ga 3p XPS spectra of the reference sample are presented in Fig. 7. Prior to the Ar^+ bombardment (Fig. 7(a)) the Ga reference sample has a native oxide, Ga_2O_3, surface layer, which is also indicated by the shoulder on the high binding energy side of the Ga $3p_{1/2}$ peak. The corresponding Ga $3p_{3/2}$ peak for the Ga_2O_3 phase is located between the primary spin–orbit components of the metallic Ga. After Ar^+ bombardment of the Ga reference sample (Fig. 7(d)) the dominating features are the metallic Ga $3p_{3/2}$ and $3p_{1/2}$ peaks at 104.1 and 107.5 eV, respectively. Note that the peak locations for Ga in metallic Ga and in both MAX phases are almost identical.

Included in Fig. 7 are also the corresponding spectra for the Mo_2GaC and Mo_2Ga_2C MAX-phases shown in Fig. 7(b) and (c), respectively. The comparison shows that the Ga in the MAX-phases is partly oxidized and that the Mo_2GaC sample is significantly more oxidized as compared to the Mo_2Ga_2C sample. Elemental quantification using the XPS spectra presented in Fig. 6 indicates that both samples consists of 20 at.% of oxygen and with a O:Ga ratio of 1.4 and 0.32 for the Mo_2GaC and Mo_2Ga_2C samples, respectively. However, the oxidation process is limited to the near surface region, which is probed by XPS, while the rest of the material is intact as evidenced by the only 0.34 at.% O determined through using ERDA [13]. Since the samples are extensively exposed to the atmosphere, it is not unreasonable to assume that oxygen penetrates into the near surface region along grain boundaries and possibly further into the Ga-layers. The more oxidized Ga single-layer will have a different work function compared to the less oxidized Ga double-layer, which will cause an upward band bending and thus a depletion of electrons from the non-oxidized components in the sample [29]. This charge transfer is observed in Fig. 6, as all Mo_2GaC spectra are shifted toward lower binding energies compared to those in the Mo_2Ga_2C phase.

This interpretation explains why the main features of the O 1s, C 1s, Mo 3d, and Ga 3p spectra for the Mo_2GaC and the Mo_2Ga_2C in Fig. 6 do not line up. The broader appearance of the Mo $3d_{5/2}$ for Mo_2GaC and the shoulder on the low binding energy side of the main $3d_{5/2}$ peak in Mo_2Ga_2C suggest that there is some double-layered Ga in Mo_2GaC and some single-layered Ga in Mo_2Ga_2C, consistent with the defects observed in Fig. 5. The additional intensity around 229.2 eV in the Mo 3d spectrum for the Mo_2Ga_2C sample reveals the presence of MoO_2 [30]. However, the most important observation is the similarity between the Mo 3d and the C1s peaks of Mo_2GaC, Mo_2Ga_2C, and Mo_2C [31], see Fig. 8, which implies that both Mo_2GaC and Mo_2Ga_2C consist of Mo_2C-layers. In fact, the XPS study confirms that there are no structural differences in the Mo_2C-layers between Mo_2GaC and Mo_2Ga_2C.

5. Conclusions

We have performed first principles calculations in combination with experimental work including NPD Rietveld refinement, HR-STEM, and XPS, to explore the structure and chemistry of Mo_2Ga_2C. The theoretical, as well as the experimental, results support the existence of a stoichiometric phase with a Ga bilayer – stacked in a simple hexagonal arrangement – between a pair of twinned Mo_2C layers. It follows that the only structural difference between Mo_2Ga_2C and the well-known Mo_2GaC MAX phase is the insertion of an additional Ga layer. Based on their similar structures and the track record of MAX phase discoveries, it is quite reasonable to assume that Mo_2Ga_2C is the first phase in a distinct family of MAX-related phases.

References

[1]   M. W. Barsoum, MAX Phases: Properties of Machinable Carbides and Nitrides, Wiley VCH GmbH & Co., Weinheim, 2013.

[2]   P. Eklund, M. Beckers, U. Jansson, H. Högberg and L. Hultman, The $M_{n+1}AX_n$ phases: Materials science and thin-film processing, *Thin Solid Films* 518 (2010) 1851.

[3]   Z. M. Sun, Progress in research and development on MAX phases: A family of layered ternary compounds, *Int. Mater. Rev.* 56 (2011) 143.

[4]   M. W. Barsoum, The $M_{N+1}AX_N$ Phases: A New Class of Solids; Thermodynamically Stable Nanolaminates, *Prog. Solid St. Chem.* 28 (2000) 201.

[5]   B. Holm, R. Ahuja, S. Li and B. Johansson, Theory of the ternary layered system Ti-Al-N, *J. Appl. Phys.* 91 (2002) 9874.

[6]   A. Grechnev, S. Li, R. Ahuja, O. Eriksson, U. Jansson and O. Wilhelmsson, Layered compound Nb_3SiC_2 predicted from first-principles theory, *Appl. Phys. Lett.* 85 (2004) 3071.

[7]   W. Luo, C. M. Fang and R. Ahuja, Nanolayered MAX Phaes from *ab initio* Calculations, *Int. J. Modern Phys. B* 22 (2008) 4495.

[8]   C. Li, J. Kuo, B. Wang, Y. Li and R. Wang, A new layer compound Nb_4SiC_3 predicted from first-principles theory, *J. Phys. D: Appl. Phys.* 42 (2009) 075404.

[9]   V. J. Keast, S. Harris and D. K. Smith, Prediction of the stability of the $M_{n+1}AX_n$ phases from first principles, *Phys. Rev. B* 80 (2009) 214113.

[10]   P. Eklund, M. Dahlqvist, O. Tengstrand, L. Hultman, J. Lu, N. Nedfors, U. Jansson and J. Rosen, Discovery of the Ternary Nanolaminated Compound Nb_2GeC by a Systematic Theoretical-Experimental Approach, *Phys. Rev. Lett.* 109 (2012) 035502.

[11]   A. S. Ingason, A. Mockute, M. Dahlqvist, F. Magnus, S. Olafsson, U. B. Arnalds, B. Alling, I. A. Abrikosov, B. Hjörvarsson, P. O. Å. Persson and J. Rosen, Magnetic Self-Organized Atomic Laminate from First Principles and Thin Film Synthesis, *Phys. Rev. Lett.* 110 (2013) 195592.

[12]   A. S. Ingason, A. Petruhins, M. Dahlqvist, F. Magnus, A. Mockute, B. Alling, L. Hultman, I. A. Abrikosov, P. O. Å. Persson and J. Rosen, A Nanolaminated Magnetic Phase: Mn$_2$GaC, *Mater. Res. Lett.* 2 (2014) 89.

[13]   C. Hu, C.-C. Lai, Q. Tao, J. Lu, J. Halim, L. Sun, J. Zhang, J. Yang, B. Anasori, J. Wang, Y. Sakka, L. Hultman, P. Eklund, J. Rosen and M. W. Barsoum, Mo$_2$Ga$_2$C: a new ternary nanolaminated carbide, *Chem. Commun.* 51 (2015) 6560.

[14]   R. Meshkian, A. S. Ingason, M. Dahlqvist, A. Petruhins, U. B. Arnalds, F. Magnus, J. Lu and J. Rosen, Theoretical stability, thin film synthesis and transport properties of the Mo$_{n+1}$GaC$_n$ MAX phase, *Phys. Status Solidi RRL* 9 (2015) 197.

[15]   P. E. Blöchl, Projector augmented-wave method, *Phys. Rev. B* 50 (1994) 17953.

[16]   G. Kresse and J. Hafner, *Ab initio* molecular dynamics for open-shell transition metals , *Phys. Rev. B* 48 (1993) 13115.

[17]   G. Kresse and D. Joubert, From ultrasoft pseudopotentials to the projector augmented-wave method, *Phys. Rev. B* 59 (1999) 1758.

[18]   G. Kresse and J. Hafner, *Ab initio* molecular-dynamics simulation of the liquid-metal–amorphous-semiconductor transition in germanium, *Phys. Rev. B* 49 (1994) 14251.

[19]   J. P. Perdew, K. Burke and M. Ernzerhof, Generalized Gradient Approximation Made Simple, *Phys. Rev. Lett.* 77 (1996) 3865.

[20]   H. J. Monkhorst and J. D. Pack, Special points for Brillouin-zone integrations, *Phys. Rev. B* 13 (1976) 5188.

[21] A. Petruhins, A. S. Ingason, M. Dahlqvist, A. Mockute, M. Junaid, J. Birch, J. Lu, L. Hultman, P. O. Å. Persson and J. Rosen, Phase stability of $Cr_{n+1}GaC_n$ MAX phases from first principles and Cr_2GaC thin-film synthesis using magnetron sputtering from elemental targets, *Phys. Status Solidi RRL* 7 (2013) 971.

[22] O. Rivin, E. N. Caspi, H. Ettedgui, H. Shaked and A. Goukassov, Magnetic structure determination of $TbCo_2Ni_3$ using polarized and nonpolarized neutron powder diffraction, *Phys. Rev. B* 88 (2013) 054430.

[23] J. R. Carvajal, Recent advances in magnetic structure determination neutron powder diffraction, *Physica B* 192 (1993) 55.

[24] M. Dahlqvist, B. Alling, I. A. Abrikosov and J. Rosen, Phase stability of Ti_2AlC upon oxygen incorporation: A first-principles investigation, *Phys. Rev. B* 81 (2010) 024111.

[25] M. Dahlqvist, B. Alling and J. Rosen, Stability trends of *MAX* phases from first principles, *Phys. Rev. B* 81 (2010) 220102.

[26] A. Mockute, M. Dahlqvist, J. Emmerlich, L. Hultman, J. M. Schneider, P. O. Å. Persson and J. Rosen, Synthesis and *ab initio* calculations of nanolaminated $(Cr,Mn)_2AlC$ compounds, *Phys. Rev. B* 87 (2013) 094113.

[27] A. Mockute, P. O. Å. Persson, F. Magnus, A. S. Ingason, S. Olafsson, L. Hultman and J. Rosen, Synthesis and characterization of arc deposited magnetic $(Cr,Mn)_2AlC$ MAX phase films, *Phys. Status Solidi RRL.* 8 (2014) 420.

[28] L. Fast, J. M. Wills, B. Johansson and O. Eriksson, Elastic constants of hexagonal transition metals: Theory, *Phys. Rev. B* 51 (1995) 17431.

[29] Z. Zhang and J. T. Yates, Jr., Band Bending in Semiconductors: Chemical and Physical Consequences at Surfaces and Interfaces, *Chem. Rev.* 112 (2012) 5520.

[30]   T. Schroeder, J. Zegenhagen, N. Magg, B. Immaraporn and H.-J. Freund, Formation of a faceted MoO_2 epilayer on Mo(1 1 2) studied by XPS, UPS and STM, *Surf. Sci.* 552 (2004) 85.

[31]   C. A. Wolden, A. Pickerell, T. Gawai, S. Parks, J. Hensley and J. D. Way, Synthesis of β-Mo_2C Thin Films, *ACS Appl. Mater. Interfaces* 3 (2011) 517.

Table 1. Calculated unit cell volume, lattice parameters, and total energies, per formula unit, for competing phases considered in the ternary Mo–Ga–C system. The values for Mo_2Ga_2C phases are listed in Table 2.

Phase	Prototype structure	Pearson symbol	Space group	V_0 (Å³/uc)	a (Å)	b (Å)	c (Å)	E_0 (eV/fu)
Mo	W	cI2	$Im\bar{3}m$ (229)	15.92	3.169			-10.850
Mo	Cu	cF4	$Fm\bar{3}m$ (225)	16.15	4.012			-10.431
Mo	Mg	hP2	$P6_3/mmc$ (194)	32.57	2.774		4.887	-10.414
Ga	α-Ga	oC8	$Cmca$ (64)	162.77	4.590	7.753	4.575	-3.030
Ga	Ga	oC4	$Cmcm$ (63)	38.43	2.795	8.114	3.380	-3.012
Ga	Ga	mC4	C2/c (15)	38.38	2.818	8.167	3.330	-3.012
C	C (graphite)	hP4	$P6_3/mmc$ (194)	38.14	2.464		7.250	-9.225
MoC	TiP	hP8	$P6_3/mmc$ (194)	84.84	3.016		10.768	-19.821
MoC	NaCl	cF8	$Fm\bar{3}m$ (225)	21.06	4.383			-19.640
MoC	η-MoC	hp12	$P6_3/mmc$ (194)	126.16	3.074		15.401	-19.747
MoC	WC	hp2	$P\bar{6}m2$ (187)	21.00	2.928		2.829	-20.241
Mo_3C_2	Cr_3C_2	oP20	$Pnma$ (62)	228.19	6.064	2.974	12.654	-50.938
Mo_2C	β''-Mo_2C	hP3	$P\bar{3}m1$ (164)	38.06	3.068		4.669	-31.064
Mo_3C	Fe_3C	oP16	$Pnma$ (62)	215.87	5.540	7.559	5.159	-40.423
Mo_6Ga_{31}	Mo_6Ga_{31}	mP148	$P2_1/c$ (14)	2647.42				-163.927
Mo_8Ga_{41}	V_8Ga_{41}	hR147	$P\bar{3}$ (148)	2625.14				-217.436
$MoGa_4$	$CrGa_4$	cI10	$Im\bar{3}m$ (229)	102.47	5.106			-23.818
$MoGa_3$	$TiAl_3$	tI8	$I4/mmm$ (139)	72.10	5.189		5.428	-18.485
$MoGa_2$	CdI_2	hP3	$P\bar{3}m1$ (164)	48.84	2.904		6.689	-16.658
Mo_2Ga_3	Ti_2Ga_3	tP10	$P4/m$ (83)	155.67	6.515		3.667	-30.851
MoGa	FeSi	cP8	$P2_13$ (198)	126.05	5.014			-13.760
Mo_5Ga_4	Ti_5Ga_4	hP18	$P6_3/mcm$ (193)	276.95	7.817		5.234	-66.314
Mo_3Ga_2	U_3Si_2	tP10	$P4/mbm$ (127)	154.78	6.784		3.363	-38.294
Mo_5Ga_3	Cr_5As_3	oP32	$Pnma$ (62)	510.53	9.839	7.807	6.639	-62.659
Mo_2Ga	Cu_2Sb	tP6	$P4/mmm$ (129)	95.73	3.682		7.062	-24.438
Mo_2Ga	Fe_2P	hP9	$P\bar{6}2m$ (189)	140.12	7.192		3.127	-24.527
Mo_5Ga_2	Mn_5Ge_2	hP42	$P3c1$ (158)	670.89				-59.508
Mo_3Ga	Cr_3Si	cP8	$Pm\bar{3}n$ (223)	123.39	4.979			-36.200
Mo_3GaC	$CaTiO_3$	cP5	$Pm\bar{3}m$ (221)	71.57	4.152			-44.274
Mo_2GaC	Cr_2AlC	hP8	$P6_3/mmc$ (194)	108.20	3.068		13.272	-34.413
Mo_3GaC_2	Ti_3SiC_2	hP12	$P6_3/mmc$ (194)	151.38	3.086		18.358	-54.040
Mo_4GaC_3	Ti_4AlN_3	hP16	$P6_3/mmc$ (194)	196.55	3.133		23.116	-73.789

Table 2 Structural and stability related information for the three crystal structures with Mo_2Ga_2C composition presented in Fig. 1. The negative values for ΔH_{cp} indicate stability relative to the set of most competing phases.

	V_0 (Å^3/uc)	a (Å)	c (Å)	E_0 (eV/uc)	ΔE_{single} (meV/atom)	ΔH_{cp} (meV/atom)
C between Mo-layers (Figure 1(a))[†]	147.59	3.064	18.153	-75.384	-142	-9
C between Ga-layers (Figure 1(b))	143.41	3.068	17.596	-67.438	+653	+786
C between Mo-layers and zig-zag stacking of Ga (Figure 1(c))[‡]	146.47	3.091	17.705	-74.057	-9	+124

[†] Identified set of most competing phases at Mo_2Ga_2C composition are Mo_3Ga, MoC, and $MoGa_4$.

[‡] Note that the space group considered for the zig-zag stacked Mo_2Ga_2C is $P\bar{3}m1$ (164).

Table 3 a and c lattice parameters and structural models of Mo_2Ga_2C obtained from the calculation (only the most stable structure, Fig. 1(a)) and from Rietveld analysis of XRD and NPD patterns.

	Calculation (Fig. 1(a))				XRD (from [13])				NPD[†]			
a (Å)	3.06396				3.03396(4)				3.03(1)			
c (Å)	18.1532				18.0814(3)				18.1(1)			
Space Group	$P6_3/mmc$				$P6_3/mmc$				$P6_3/mmc$			
	Wyckoff Notation	x	y	z	Wyckoff Notation	x	y	z	Wyckoff Notation	x	y	z
Mo	4f	1/3	2/3	0.06489	4f	1/3	2/3	0.06571(11)	4f	1/3	2/3	0.065(8)
Ga	4f	1/3	2/3	0.68132	4f	1/3	2/3	0.68247(13)	4f	1/3	2/3	0.69(1)
C	2a	0	0	0	2a	0	0	0	2a	0	0	0

Table 4 Calculated elastic constants C_{ij}, bulk moduli B_V, shear moduli G_V, Young's moduli E, Poisson´s ratio v, and the anisotropy factor A for Mo$_2$Ga$_2$C (Fig. 1(a)) and Mo$_2$GaC.

Phase	C_{11} (GPa)	C_{12} (GPa)	C_{13} (GPa)	C_{33} (GPa)	C_{44} (GPa)	B_V (GPa)	G_V (GPa)	E (GPa)	v	A
Mo$_2$Ga$_2$C	244	62	108	341	78	154	86	218	0.26	0.85
Mo$_2$GaC	294	96	161	289	126	190	101	257	0.28	1.93
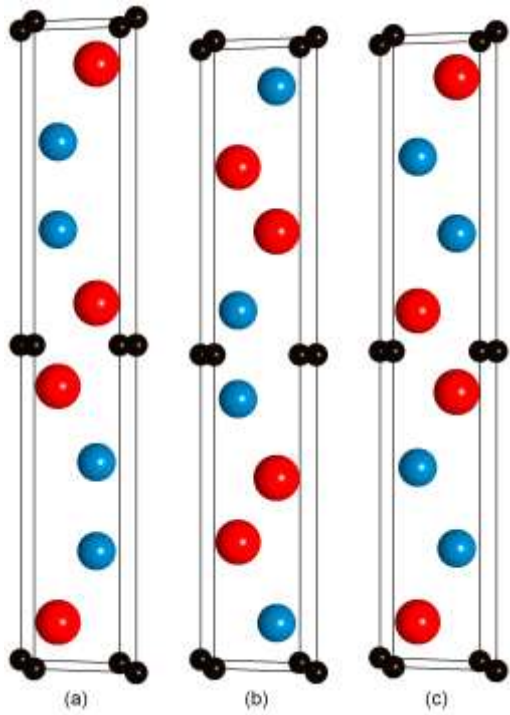
Fig. 1. Crystal structures of Mo_2Ga_2C composition with (a) C atoms between the Mo-layers, (b) C atoms between Ga-layers, and (c) C a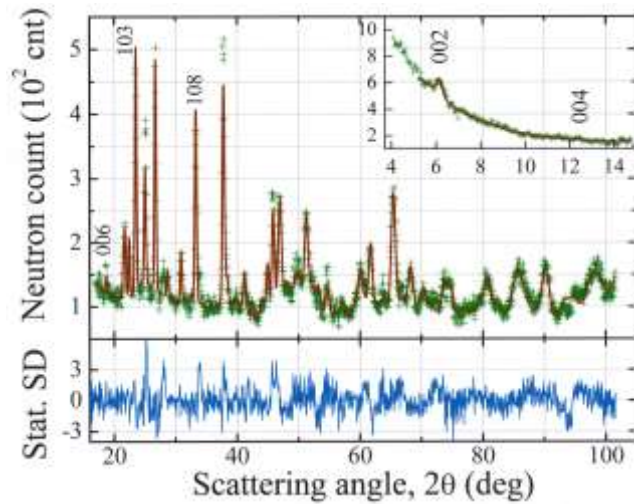toms between Mo-layer but a zig-zag stacking of the Ga atoms, where the Mo atoms are in red, Ga in blue and C in black. All illustrations are scaled accordingly to their actual structure sizes.
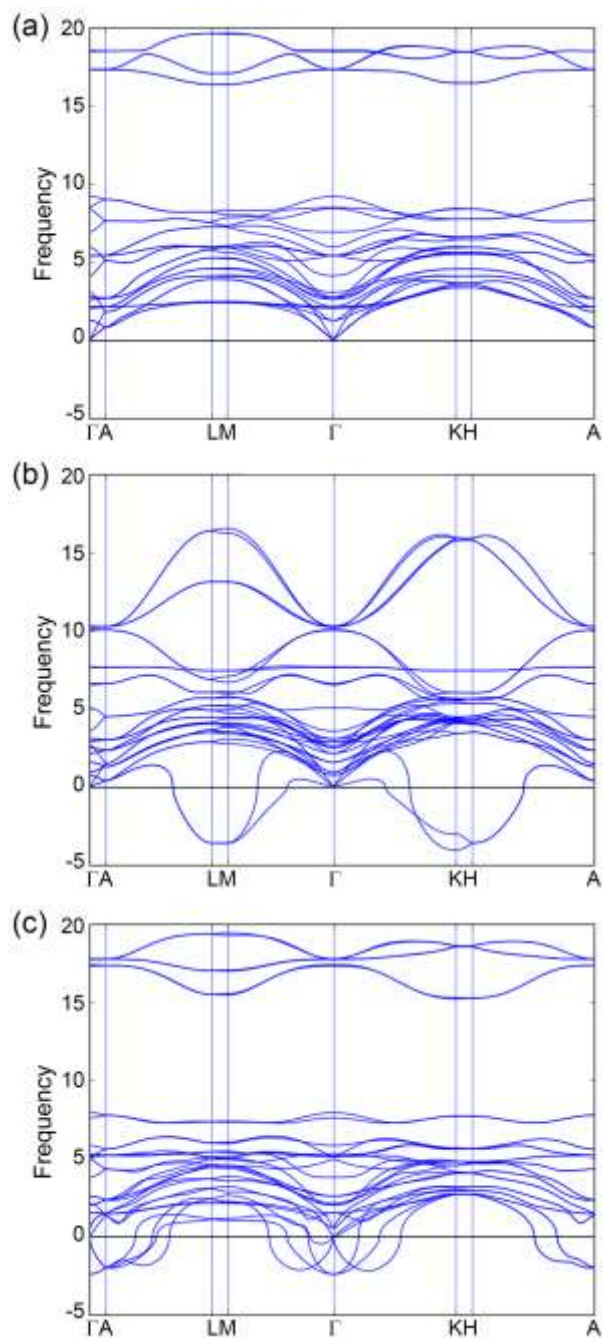
Fig. 2. Dynamical stability of Mo$_2$Ga$_2$C composition with (a) C atoms between the Mo-layers, (b) C atoms between Ga-layers, and (c) C atoms between Mo-layer but a zig-zag stacking of the Ga atoms.

Fig. 3. NPD of Mo_2Ga_2C, observed at room temperature (crosses) as a function of scattering angle, 2θ. The Rietveld refined NPD profile (top) is shown to fit the observed count, determined by the difference between the observed and refined profiles (bottom), normalized by the statistical uncertainty in the observed count (see text). The inset at the top-right corner presents the low-angle count. Selected reflections are denoted using their Miller indices.
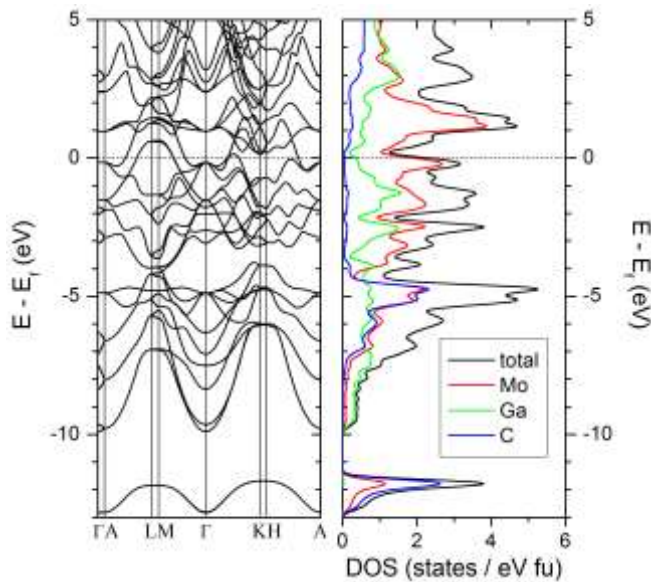
Fig. 4. Calculated electronic band structure (left) and density of states (right) for Mo_2Ga_2C for the structure shown in Fig. 1(a). The Fermi level is indicated by the horizontal dashed line.
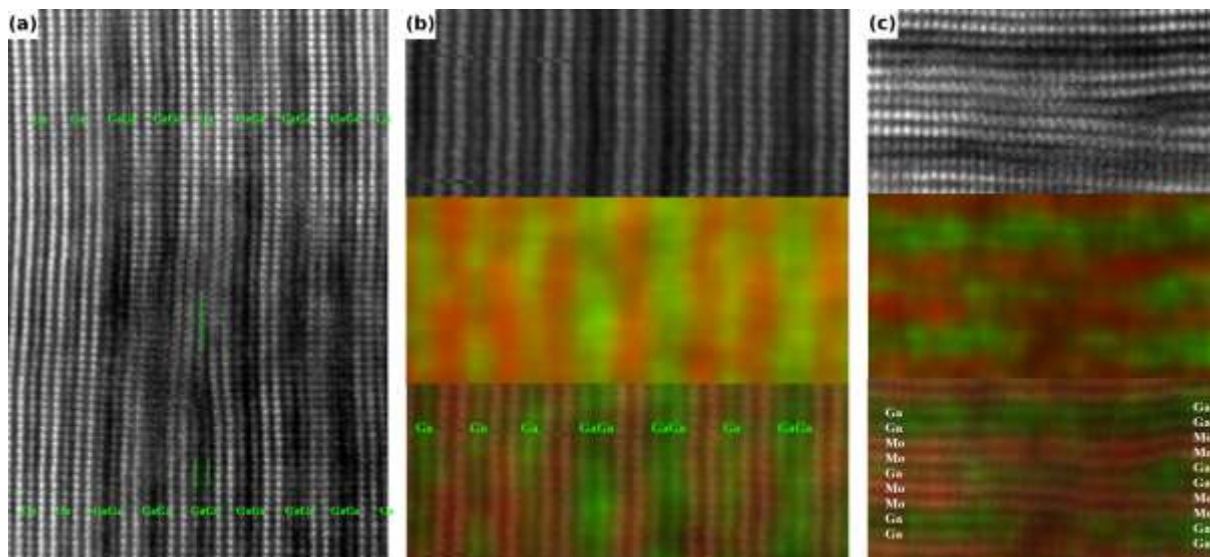
Fig. 5. (a) STEM image of Mo_2Ga_2C phase acquired along its [210] zone axis, where the Ga layers are highlighted with green 'Ga' labels and lines. (b and c) STEM images (top), $Mo + Ga$ EDX mappings (center), and superimposed STEM images and $Mo + Ga$ EDX mappings (bottom) of Mo_2Ga_2C phase acquired along the [210] zone axis.

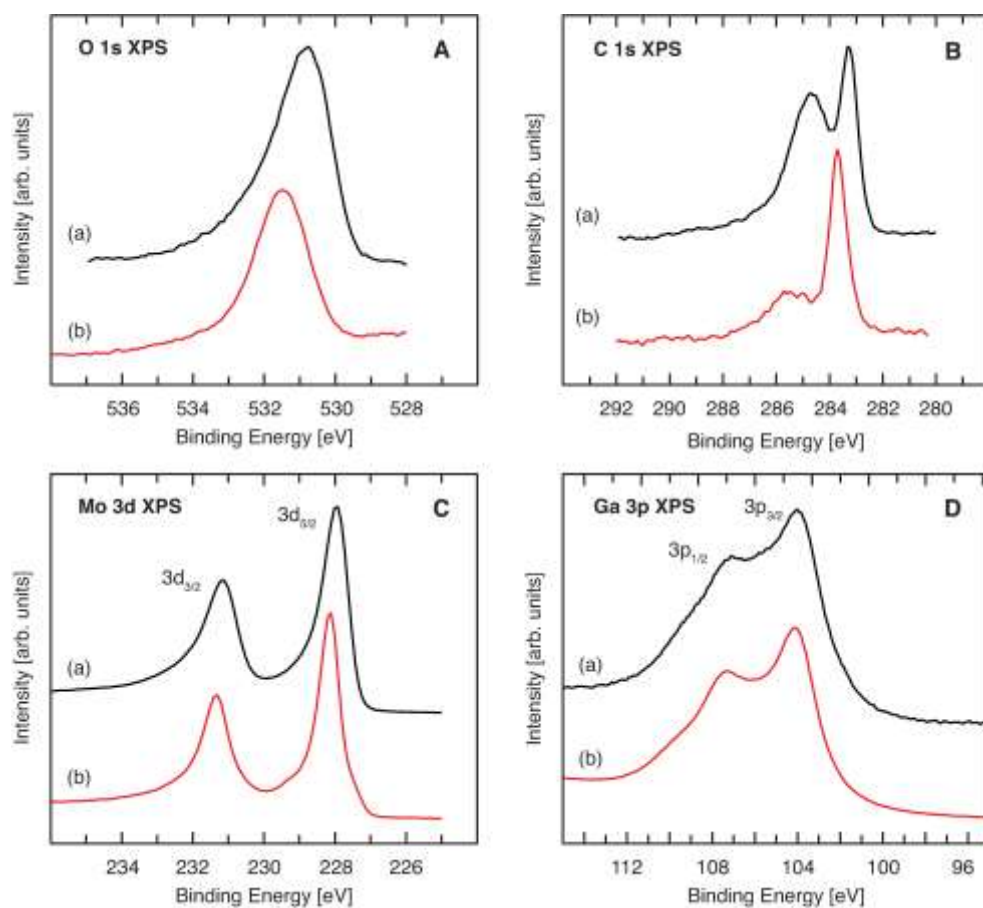**Fig. 6.** XPS spectra for (a) Mo$_2$GaC and (b) Mo$_2$Ga$_2$C. Panels (A)–(D) show the O 1s, C 1s, Mo 3d, and Ga 3p regions, respectively.
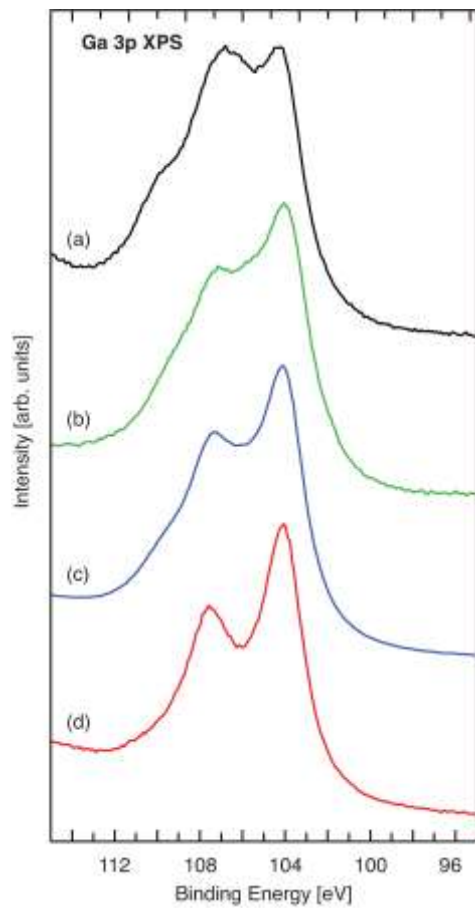
Fig. 7. Ga 3p XPS spectra for (a) metallic Ga with native Ga_2O_3 surface layer, (b) Mo_2GaC, (c) Mo_2Ga_2C, and (d) metallic Ga after 500 eV Ar^+ bombardment.
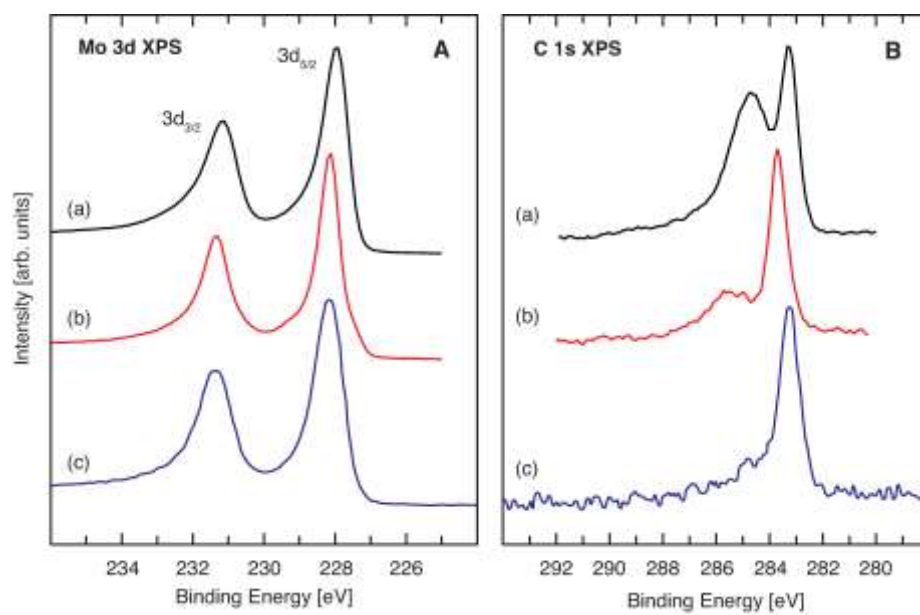
Fig. 8. XPS spectra for (a) Mo$_2$GaC, (b) Mo$_2$Ga$_2$C, and (c) β-Mo$_2$C obtained from Ref. [31].

Panels (A) and (B) show the Mo 3d and C 1s regions, respectively.